Theor Chem Acc (2012) 131:1169
DOI 10.1007/s00214-012-1169-z

REGULAR ARTICLE

Numerical integration of atomic electron density with double exponential formula for density functional calculation

Masaki Mitani · Yasunori Yoshioka

Received: 14 October 2011 / Accepted: 27 December 2011 / Published online: 28 February 2012

Abstract In the preceding study, we reported an application of the double exponential formula to the radial quadrature grid for numerical integration of the radial electron distribution function. Three-type new radial grids with the double exponential transformation were introduced. The performance of radial grids was compared between the double exponential grids and the grids proposed in earlier studies by applying to the electron-counting integrals of noble gas atoms and diatomic molecules including alkali metals, halogens, and transition metals. It was confirmed that the change in accuracy of the quadrature approximation depending on atomic or molecular species is not significant for the double exponential integration schemes rather than the other integration schemes. In the present study, we further investigate the accuracy of the double exponential formula for the electron-counting integrals of all the atoms from H to Kr in the periodic table to elucidate the stable performance of the double exponential radial grids. The electron densities of the atoms are calculated with the Gauss-type orbital basis functions at the B3LYP level. The quadrature accuracy and convergence behavior of numerical integration are compared among the double exponential formula and the formulas proposed by Treutler et al. and by Mura et al. The results reveal that the double exponential radial grids remarkably improve the convergence rate toward high accuracy compared with the previous radial grids, particularly for heavy elements in the 4th period, without fine tuning of the radial grids for each atom.

Keywords Double exponential formula · Numerical integration · Quadrature grid · Electron-counting integral · Density functional calculation

1 Introduction

In Kohn–Sham density functional theory (DFT) calculations, the energy components of a molecule for the exchange and correlation terms are calculated by numerical integration of the approximated functional represented with electron density and its derivatives. Since quadrature grid points surrounding a molecule are used to perform the numerical integration, the accuracy of integrated result depends on the number and distribution of the grid points. The integrated values approach the exact value with increasing the number of grid points to infinity, while the use of a large-size grid requires a long computation time. It is, therefore, desired to develop an integration scheme which enables us to obtain accurate results with the smallest possible quadrature grid for large-scale and/or long-time DFT applications such as dynamics simulation of biomolecules or materials.

Becke has introduced a fuzzy cell method to the numerical integration of multi-center functions [1]. The multi-center integrand for a molecule $F(\vec{r})$ is decomposed into a sum of the single-center integrands for each atom $F_A(\vec{r})$ by using a nuclear weight function $w_A(\vec{r})$ such as Eqs. 1–3. Thus, the multi-center integral can be reduced to a sum of the single-center integrals as given in Eq. 4. The nuclear weight function is calculated at every grid point in a quadrature approximation.

Electronic supplementary material The online version of this article (doi:10.1007/s00214-012-1169-z) contains supplementary material, which is available to authorized users.

M. Mitani (✉) · Y. Yoshioka
Department of Chemistry for Materials,
Graduate School of Engineering, Mie University,
1577 Kurima-machiya, Tsu, Mie 514-8507, Japan
e-mail: mitani@chem.mie-u.ac.jp

$$F(\vec{r}) = \sum_A F_A(\vec{r}) \tag{1}$$

$$F_A(\vec{r}) = w_A(\vec{r})F(\vec{r}) \tag{2}$$

$$\sum_A w_A(\vec{r}) = 1 \tag{3}$$

$$I = \int F(\vec{r})\mathrm{d}^3\vec{r} = \sum_A \int F_A(\vec{r})\mathrm{d}^3\vec{r} = \sum_A I_A \tag{4}$$

The single-center integration for Eq. 4 is carried out in the spherical polar coordinate system centered on the nucleus of an atom as follows.

$$I_A = \int_0^\infty \int_0^\pi \int_0^{2\pi} F_A(r_A, \theta_A, \phi_A) r_A^2 \mathrm{d}r_A \sin\theta_A \mathrm{d}\theta_A \mathrm{d}\phi_A \tag{5}$$

The three-dimensional integral of Eq. 5 is evaluated by successive numerical integration for the two-dimensional angular variables $\Omega = (\theta, \phi)$ and for the one-dimensional radial variable r. By applying the n-point quadrature formula with the weight w for grid points (n^Ω and w^Ω for angular grid and n^r and w^r for radial grid), the angular and radial integrals are approximated by Eqs. 6 and 7, respectively.

$$\begin{aligned}\bar{F}_A(r_A) &= \int_0^\pi \int_0^{2\pi} F_A(r_A, \theta_A, \phi_A) \sin\theta_A \mathrm{d}\theta_A \mathrm{d}\phi_A \\ &\approx \sum_{i=1}^{n_A^\Omega} w_i^\Omega F_A(r_A, \Omega_i)\end{aligned} \tag{6}$$

$$\bar{I}_A = \int_0^\infty \bar{F}_A(r_A) r_A^2 \mathrm{d}r_A \approx \sum_{i=1}^{n_A^r} w_i^r \bar{F}_A(r_i) \tag{7}$$

Concerning numerical integration for the angular part of Eq. 6, Lebedev grid [2] is frequently employed as a quadrature grid. The sampling points of Lebedev grid are distributed on the surface of a unit sphere so as to be invariant under the octahedron group with inversion. Various sizes of Lebedev grid have been developed from the 6-point to 5810-point grids at present [2–7]. Each of Lebedev grids can accurately integrate all the spherical harmonics and all the squares of spherical harmonics, respectively, up to a given maximum angular momentum of $l_{\max 1}$ and $l_{\max 2}$: for example, $l_{\max 1} = 5$ and $l_{\max 2} = 2$ for the 14-point grid, $l_{\max 1} = 11$ and $l_{\max 2} = 5$ for the 110-point grid, $l_{\max 1} = 21$ and $l_{\max 2} = 10$ for the 170-point grid, $l_{\max 1} = 31$ and $l_{\max 2} = 15$ for the 350-point grid, $l_{\max 1} = 41$ and $l_{\max 2} = 20$ for the 590-point grid, and $l_{\max 1} = 53$ and $l_{\max 2} = 26$ for the 974-point grid. Lebedev grids are available in quantum chemistry programs such as Gaussian, NWChem, Q-Chem, Gamess, and so on.

On the other hand, regarding numerical integration for the radial part of Eq. 7, many different schemes have been introduced [1, 8–20]. In earlier studies, the Gauss–Chebyshev formula or the Euler-Mclaurin formula was used as a quadrature rule [1, 8, 9, 11, 12]. In recent studies, a multi-exponential grid [17] and a basis set adaptive grid [20] were proposed as an efficient radial grid. The multi-exponential grid adopted the log-squared quadrature rule [17]. The basis set adaptive grid directly applied the Gauss–Legendre quadrature and the Gauss-Laguerre quadrature to finite integrals and a semi-infinite integral, respectively, by dividing semi-infinite region of the radial integral into finite intervals and a semi-infinite interval [20]. The comparisons of performance for some of these radial grids have been reported [10, 12, 16, 17, 19–21]. The radial integration is carried out by combining a quadrature rule with a variable transformation to map the variable of the quadrature grid on the variable of the radial grid. The mapping transformation includes an adjustable parameter that varies the distribution of sampling points. Consequently, the integrated results also depend on the mapping parameter specific to each atom. Since the best value of the mapping parameter would differ for an isolated atom and for an atom in molecules, the wide range of sweet spot for the mapping parameter is one of the desirable properties of a radial grid for stable integration of atomic and molecular integrals. The optimal values of the mapping parameter were proposed for each of the radial grids [1, 8, 9, 11, 12, 21, 22].

In addition, a grid pruning technique has been considered to reduce the number of sampling points for numerical integration [8, 9, 11, 12, 21, 22]. Since the electron density distribution in a molecule is almost spherically symmetric in the vicinity of the nucleus of a given atom, small-size angular grids can be used for the radial points in core region with acceptable loss of accuracy. The grid pruning assigns a different angular grid to each of radial points instead of applying common angular grid to all the radial points based on the position of radial points such as core, middle, and outer regions. The radial grid can be also pruned for the radial points far from an atomic nucleus, since the contribution of such points to the integrand is negligible. The most of standard fixed grids employed in popular DFT codes are pruned for efficiency.

The sensitivity of molecular properties to the integration grid sizes has been investigated with Gaussian, Molpro, NWChem, Q-Chem, and Gamess [23–25]. The problems associated with the standard grids were pointed out as follows. Spurious negative eigenvalues in the Hessian matrix or artificial loss of vibrational mode degeneracy arose from the application of pruned coarse grids to the coupled perturbed Kohn–Sham equation [23]. Fine-meshed grids appropriate for typical first- and second-row systems

were not suitable for systems involving very heavy elements such as third-row transition metals [23]. The meta-generalized gradient approximation (meta-GGA) for density functionals using the standard grids predicted oscillations and multiple minima in the potential energy surfaces of some dispersion-bound dimers [24]. Increasing the integration grid size made the potential energy surfaces smoother but not necessarily single-minimum [24]. The energetic errors for alcohols and thioalcohols suggested that few of these molecules could be computed precisely by the BLYP method with a large grid [25]. Pathological cases with poor precision increased for the non-Abelian molecules in the search for higher precision through use of a larger grid [25]. Although the problems mentioned above will be avoided by using a much larger grid, unacceptably long time may be required for computation. It is, thus, needed to develop the radial and angular grids for efficient integration which give results of the highest precision with the minimum sampling points. In other words, the integration grids should have a property that the integrated values converge as fast as possible to the exact value by increasing the grid points for all the atomic species.

Double exponential (DE) formula has been proposed as an efficient numerical integration scheme by Takahashi and Mori [26]. The error of the DE formula is analytically expressed in the form of $O(\exp(-cN/\log N)$, where N is the number of sampling points and c is a positive constant. Therefore, the DE scheme is expected to provide fast convergence of numerical integration as N becomes large. The DE quadrature adopts the equally meshed trapezoidal rule as a quadrature rule for numerical integration after an integral over arbitrary intervals is transformed into an infinite integral by variable transformation. The variable transformation in the DE integration is designed as follows that the transformed integrand decays double exponentially near the end points of the transformed interval of integration. A variety of the DE transformations have been proposed according to the type of integral for finite, semi-infinite, and infinite integrals [26–31].

In the preceding paper, we have applied the DE formula to numerical integration of the radial part given in Eq. 7 [32]. Three-type DE transformations were introduced to derive new radial grids. Since it is obvious that the exact solution is total electron number, the integration of electron density (electron-counting integral) for atomic and diatomic molecular systems was examined with respect to the noble gas atoms of He, Ne, Ar, and Kr and the diatomic molecules of LiH, NaH, KH, Li_2, Na_2, K_2, HF, HCl, HBr, F_2, Cl_2, Br_2, LiF, NaCl, KBr, $[ScH]^+$, $[MnH]^+$, and $[CuH]^+$ as test cases. The performance of various radial grids was compared in the case of atomic integrals for the grids proposed in earlier studies [1, 8, 11, 12, 17, 20] as well as for the DE grids. The previous grids of Becke (B grid) [1], Murray, Handy, and Laming (MHL grid) [8], Treutler and Ahlrichs (TA grid) [11], Mura and Knowles (MK grid) [12], Gill and Chien (MultiExp grid) [17], and Kakhiani, Tsereteli, and Tsereteli (AQR grid) [20] were examined. As for the atomic integrals, the TA, MK, and DE grids indicated higher accuracy than the B, MHL, and MultiExp grids. The convergence behavior of the accuracy for numerical integration with increasing the number of radial grid points was also compared in the case of molecular integrals among the TA, MK, and DE grids. Fast convergence to the exact value was achieved by using the DE formula, especially for the systems including heavy elements. Although more grid points were needed to obtain high accuracy by replacing an atom in a diatomic molecule from light to heavy elements, the slow convergence depending on the molecular species was more significant for the TA and MK grids than for the DE grids. The TA and MK grids gave poor results, even if the fine grid with 200 points was used, for ionically bonded molecules of alkali metal hydrides, alkali metal halogenides, and transition metal hydride cations, in contrast to the DE grids converged to the exact value. The performance of the TA and MK grids became poorer for the K-, Br-, and Sc-containing molecules compared with the other molecules in particular, whereas the DE grids demonstrated high accuracy within the 200-point grid for all the systems examined without fine tuning of the mapping parameter for each atom.

The purpose of the present paper is to further investigate the accuracy of the TA, MK, and DE radial grids for the electron-counting integrals of all the atoms from H to Kr in the periodic table to elucidate the stable performance of the DE formula. Since it has been reported that the error in the integration of electron density is a reliable guide to the error expected for the exchange and correlation energies [8, 11], accurate integration of the electron-counting integral is important. The accuracy of numerical integration for molecular integrals is affected not only by radial grid with a mapping parameter but also by angular grid and nuclear weight function. However, the examination of accuracy for atomic integrals is valuable as a guideline, since poor performance of a radial grid in atomic cases will be reflected in molecular cases. The electron density of the atoms is calculated using the Gauss-type orbital (GTO) basis functions. The accuracy and convergence of the DE grids are compared with those of the TA and MK grids. The dependence of accuracy on the mapping parameter is also given for the DE grids in relation to the stability of the DE formula.

2 TA, MK, and DE radial grids

In this section, we briefly summarize the radial grids of TA [11], MK [12], and DE [26] formulas. The radial grid to numerically integrate the radial part given in Eq. 7 is

generated with the combination of a quadrature rule and a mapping transformation $r = \alpha t(x)$ including a mapping parameter α. The Gauss–Chebyshev integration formula of the second kind given by Eqs. 8 and 9 and the Euler-Maclaurin summation formula (actually, the extended trapezoidal formula) given by Eqs. 10 and 11 have been used frequently as the n-point quadrature rule in the previous studies [1, 8–13, 18, 21].

$$\int_{-1}^{1} (1-x^2)^{1/2} f(x)\mathrm{d}x \approx \frac{\pi}{n+1}\sum_{i=1}^{n} \sin^2\left(\frac{i\pi}{n+1}\right) f(x_i) \tag{8}$$

$$x_i = \cos\left(\frac{i\pi}{n+1}\right) \tag{9}$$

$$\int_{0}^{1} f(x)\mathrm{d}x \approx \frac{1}{n+1}\sum_{i=1}^{n} f(x_i) \tag{10}$$

$$x_i = \frac{i}{n+1} \tag{11}$$

Treutler and Ahlrichs confirmed that the best performance is obtained by combining the transformation of Eq. 12 with the quadrature rule of Eqs. 8 and 9 (TA grid) [11].

$$t(x) = -\frac{(1+x)^{0.6}}{\ln 2}\ln\left(\frac{1-x}{2}\right) \tag{12}$$

The TA radial grid is given by Eqs. 13–15. The optimized values of the mapping parameter α for the TA radial grid were reported for atoms H through to Kr [11].

$$\begin{aligned}\int_{0}^{\infty} F(r)r^2\mathrm{d}r \approx \left(\frac{\alpha}{\ln 2}\right)^3 \frac{\pi}{n+1}\sum_{i=1}^{n} (1+x_i)^{1.8} \\ \times \left\{\frac{(1+x_i)^{1/2}}{(1-x_i)^{1/2}}\ln^2\left(\frac{1-x_i}{2}\right)\right. \\ \left. -0.6\frac{(1-x_i)^{1/2}}{(1+x_i)^{1/2}}\ln^3\left(\frac{1-x_i}{2}\right)\right\} F(r_i)\end{aligned} \tag{13}$$

$$r_i = -\alpha\frac{(1+x_i)^{0.6}}{\ln 2}\ln\left(\frac{1-x_i}{2}\right) \tag{14}$$

$$\begin{aligned}w_i = \left(\frac{\alpha}{\ln 2}\right)^3 \frac{\pi}{n+1}(1+x_i)^{1.8}\left\{\frac{(1+x_i)^{1/2}}{(1-x_i)^{1/2}}\ln^2\left(\frac{1-x_i}{2}\right)\right. \\ \left. -0.6\frac{(1-x_i)^{1/2}}{(1+x_i)^{1/2}}\ln^3\left(\frac{1-x_i}{2}\right)\right\}\end{aligned} \tag{15}$$

Mura and Knowles concluded that the transformation of Eq. 16 combined with the quadrature rule of Eqs. 10 and 11 produces the most suitable grid for the radial integration (MK grid) [12].

$$t(x) = -\ln\left(1-x^3\right) \tag{16}$$

The MK radial grid is given by Eqs. 17–19. The recommended values of the mapping parameter α for the MK grid were proposed for atoms H through to Zn [12].

$$\int_{0}^{\infty} F(r)r^2\mathrm{d}r \approx 3\alpha^3\frac{1}{n+1}\sum_{i=1}^{n}\frac{x_i^2\ln^2\left(1-x_i^3\right)}{1-x_i^3}F(r_i) \tag{17}$$

$$r_i = -\alpha\ln\left(1-x_i^3\right) \tag{18}$$

$$w_i = 3\alpha^3\frac{1}{n+1}\frac{x_i^2\ln^2\left(1-x_i^3\right)}{1-x_i^3} \tag{19}$$

The double exponential (DE) formula introduced by Takahashi and Mori [26] applies the uniformly divided trapezoidal rule with mesh size h to an infinite integral. A given integral over an arbitrary interval from a to b is, therefore, transformed to an integral over the interval from $-\infty$ to ∞ by suitable variable transformation of $y = t(x)$.

$$\int_{a}^{b} f(y)\mathrm{d}y = \int_{-\infty}^{\infty} f(t(x))\frac{\mathrm{d}t(x)}{\mathrm{d}x}\mathrm{d}x \approx h\sum_{-\infty}^{\infty} t'(x_i)f(t(x_i)) \tag{20}$$

$$x_i = ih \tag{21}$$

The mapping transformation such that the transformed integrand decays double exponentially at $x \to \pm\infty$ is adopted in the DE formula. Consequently, the infinite summation appeared in Eq. 20 can be truncated appropriately in actual calculations.

The practical DE transformations have been proposed for the finite, semi-infinite, and infinite integrals, respectively [26–31]. As for the semi-infinite integral with the interval of $a = 0$ and $b = \infty$, three-type transformations were introduced. We apply Eqs. 22–24 as the DE transformations for radial function in the parameter-depending forms (α in Eqs. 22–24 is a variable) instead of the original forms (α is a constant such as $\alpha = \pi/2$ or 2 or π for Eq. 22, $\alpha = 1$ or 1/2 for Eq. 23, and $\alpha = \pi/2$ for Eq. 24). Hereafter, the quadrature grids using Eqs. 22–24 are referred to as the DE1, DE2, and DE3 radial grids, respectively.

$$t(x) = \exp(\alpha\sinh x) \tag{22}$$

$$t(x) = \exp(\alpha x - \exp(-x)) \tag{23}$$

$$t(x) = \ln(\exp(\alpha\sinh x) + 1) \tag{24}$$

The DE transformations of Eqs. 22–24 combined with the trapezoidal rule of Eqs. 20 and 21 lead to the DE1, DE2, and DE3 radial grids represented by Eqs. 25–27, 28–30, and 31–33, respectively.

$$\int_{0}^{\infty} F(r)r^2\mathrm{d}r \approx h\sum_{i=-\infty}^{\infty}\alpha\exp(3\alpha\sinh x_i)\cosh x_i F(r_i) \tag{25}$$

$$r_i = \exp(\alpha\sinh x_i) \tag{26}$$

$$w_i = h\alpha \exp(3\alpha \sinh x_i) \cosh x_i \tag{27}$$

$$\int_0^\infty F(r) r^2 \mathrm{d}r \approx h \sum_{i=-\infty}^{\infty} \exp(3\alpha x_i - 3\exp(-x_i)) \times (\alpha + \exp(-x_i)) F(r_i) \tag{28}$$

$$r_i = \exp(\alpha x_i - \exp(-x_i)) \tag{29}$$

$$w_i = h \exp(3\alpha x_i - 3\exp(-x_i))(\alpha + \exp(-x_i)) \tag{30}$$

$$\int_0^\infty F(r) r^2 \mathrm{d}r \approx h \sum_{i=-\infty}^{\infty} \ln^2(\exp(\alpha \sinh x_i) + 1) \times \frac{\exp(\alpha \sinh x_i)\alpha \cosh x_i}{\exp(\alpha \sinh x_i) + 1} F(r_i) \tag{31}$$

$$r_i = \ln(\exp(\alpha \sinh x_i) + 1) \tag{32}$$

$$w_i = h \ln^2(\exp(\alpha \sinh x_i) + 1) \frac{\exp(\alpha \sinh x_i)\alpha \cosh x_i}{\exp(\alpha \sinh x_i) + 1} \tag{33}$$

3 Computational details

In this study, the electron-counting integrals for all the atoms from H to Kr (all the elements of the 1st, 2nd, 3rd, and 4th periods) in the periodic table were examined by using the TA, MK, and DE grids to compare the performance of these radial grids. Therefore, the single-center integrand $F_A(\vec{r})$ in Eq. 5 is the electron density of an atom $\rho_A(\vec{r})$. The 14-point Lebedev grid ($n^\Omega = 14$) was adopted as an angular grid, since a small size of angular grid is sufficient to numerically integrate the spherically symmetric angular part in atomic cases. To confirm the convergence behavior of the accuracy for quadrature approximation, the number of radial grid points was varied by 10 from $n^r = 30$ to $n^r = 200$ for the TA, MK, and DE radial grids.

The values of mapping parameter α for each of the TA and MK radial grids have been given for atoms H through to Kr and for atoms H through to Zn, respectively [11, 12]. The α value of the TA grid is ranging from 0.8 to 1.8 depending on atomic species [11]. The α value of the MK grid is 5.0 or 7.0 depending on the group in the periodic table [12]. The mapping parameters of alkali metals and alkaline earth metals have larger values than those of the other elements for the TA and MK grids. The reported values of α were used in numerical integration for each atom. Concerning the MK grid, we adopted $\alpha = 5.0$ for Ga–Kr atoms, since $\alpha = 7.0$ and $\alpha = 5.0$ have been applied to the elements of the groups I (except for H atom) and II and to the elements of the other groups, respectively [12]. As for the DE radial grids, the dependence of integrated results on the variation of the mapping parameter α was confirmed for each atom by increasing the mapping parameter by 0.1 from $\alpha = 0.5$ to $\alpha = 5.5$. However, the fine tuning of the DE radial grids for each atom was not carried out. We simply selected the common value of the mapping parameter to atoms H through to Kr as follows. First, average value of the accuracies over the 30-point to 200-point radial grids was calculated for each atom with a given value of the mapping parameter. Next, average value of the grid-averaged accuracies over all the atoms was further obtained. The value of the mapping parameter which gives the highest average accuracy was chosen on the basis of the atom-averaged accuracies as $\alpha = 2.4$ for the DE1 grid, $\alpha = 1.9$ for the DE2 grid, and $\alpha = 2.3$ for the DE3 grid.

The infinite summation of the DE formula appeared in Eqs. 25, 28, and 31 was approximated by the finite sum of the quadrature points corresponding to the radial points distributed from $r = 10^{-7}$ to $r = 10R$, where R denotes the atomic radius. We applied the expectation value of orbital radius for the outer valence orbital of each atom to the value of R. The analytic value of 1.5 Bohr for H atom and the theoretical values for the other atoms determined from the Hartree–Fock calculations with the primitive Slater-type orbital (STO) basis functions [33] were used.

The electron density of the atoms was computed at the DFT level approximated with the B3LYP functional for the exchange and correlation terms [34, 35] in the restricted or unrestricted form using the contracted GTO basis functions. The 6-31G basis set [36–45] and the VDZ basis set [46] were employed as the basis functions for H–Ca and Ga–Kr atoms and for Sc–Zn atoms, respectively. The SCF atomic orbitals were extracted from the formatted checkpoint file obtained from Gaussian03 program [47]. The exact value of the electron-counting integral is the number of electrons for a given atom. Each of the occupied atomic orbitals was renormalized to ensure that the exact numerical integration gives the exact electron number.

The accuracy of numerical integration was measured by the following index introduced in Ref. [17].

$$\text{Accuracy} = -\log_{10}\left|\frac{\text{Approx}}{\text{Exact}} - 1\right| \tag{34}$$

This index represents the quality of a quadrature approximation (Approx) of an integral compared with the exact value (Exact) which essentially gives the number of correct digits in the quadrature estimation. The upper limit of the accuracy defined by Eq. 34 is 15.7 calculated by logarithm of the machine epsilon in double precision of Fortran 90.

4 Results and discussion

The changes in accuracy of the TA, MK, and DE radial grids depending on atomic species are shown in Fig. 1 for

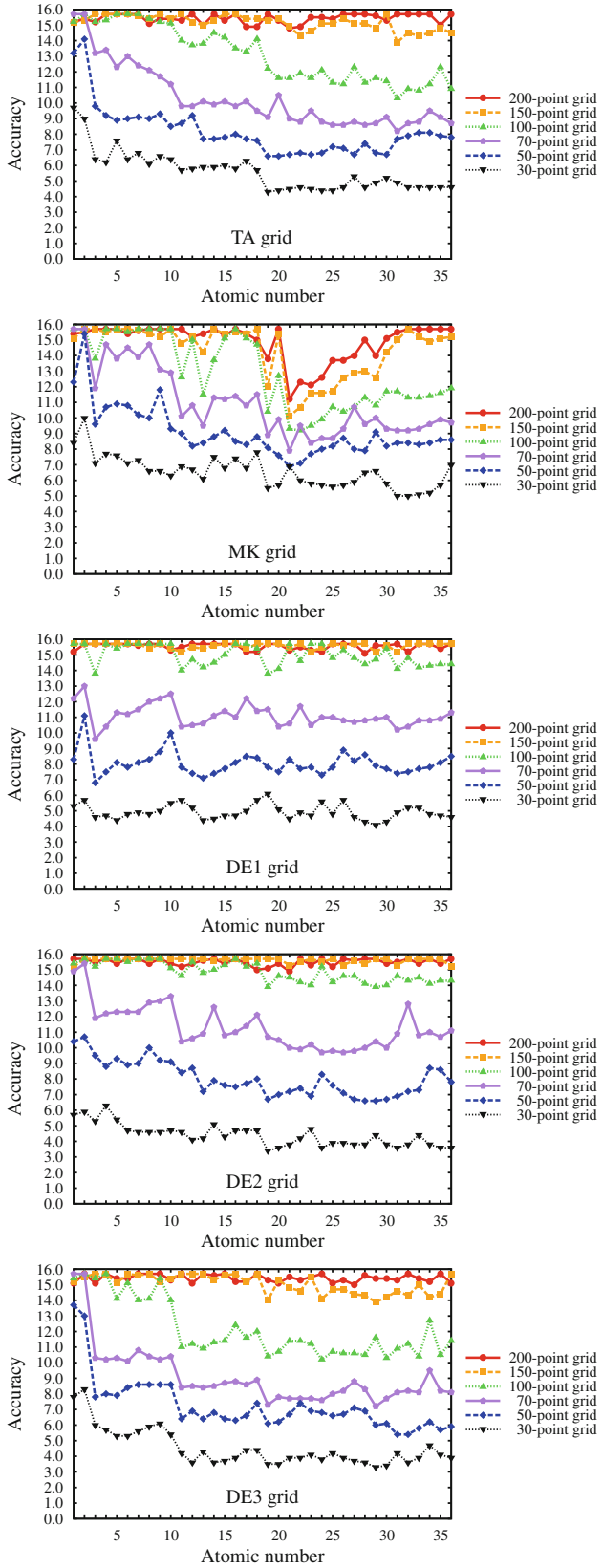

Fig. 1 Changes in accuracy of the TA, MK, DE1, DE2, and DE3 radial grids combined with Lebedev angular grid ($n^{\Omega} = 14$) for the electron-counting integrals of atoms H through to Kr

numerical integration of the atomic electron density. The plots using the selected grid sizes of $n^r = 30$, 50, 70, 100, 150, and 200 are depicted for clarity. The full lists of the accuracy with $n^r = 30$–200 are also given in Online Resources 1, 2, 3, 4, and 5 for each radial grid as Table S1 for the TA grid, Table S2 for the MK grid, Table S3 for the DE1 grid, Table S4 for the DE2 grid, and Table S5 for the DE3 grid, respectively.

Different behavior of radial grids is confirmed from Fig. 1 with respect to the convergence property of accuracy. The accuracies of the TA, DE1, DE2, and DE3 grids converge to high accuracy around 14 or 15 for all the atoms by the use of the 150-point grid, whereas the accuracies of the MK grid stay low precision for specific atoms even if the 200-point grid is employed. The TA, MK, DE2, and DE3 schemes attain fast convergence for the 1st-period elements without shell structure of the radial electron distribution in comparison with the other elements, while such fast convergence is not found for the DE1 scheme. The convergence of the TA grid becomes slow depending on the period to which integrated atoms belong. For example, the TA results using the 100-point grid indicate the accuracies such as the values around the machine precision for the 2nd-period elements, the values around 14 for the 3rd-period elements, and the values around 11 or 12 for the 4th-period elements. The performance of the MK grid largely depends on the atomic species. For instance, the MK results with the 100-point grid give remarkably low accuracies for the atoms of Li, Na, Al, and Si and for the atoms of the 4th period in contrast to the other atoms. The sensitivity for the convergence of accuracy to atomic species found in the TA and MK results is not significant for the DE1 and DE2 grids. The DE1 and DE2 results converge to the accuracy higher than 14 for all the atoms from H to Kr at $n^r = 100$. On the other hand, the DE3 results show the atom-dependent accuracy such that the accuracies of the 3rd- and 4th-period elements decrease considerably compared with those of the 1st- and 2nd-period elements at $n^r = 100$.

As mentioned above, the convergence behavior of accuracy differs for each of radial grids. To clarify the characteristic features of convergence behavior in detail, the smallest number of radial grid points required by the TA, MK, and DE schemes to obtain the exact value with the accuracy >15 is listed in Table 1 for all the atoms. The results of Table 1 are extracted from Tables S1, S2, S3, S4, and S5 given as Online Resources 1, 2, 3, 4, and 5.

The TA and MK grids need the following grid points for the elements in each period: 70 (1st period), 90–100 (2nd period), 110–120 (3rd period), and 130–170 (4th period) for the TA grid; 50–70 (1st period), 80–130 (2nd period), 90–180 (3rd period), and 140–200 (4th period) for the MK grid. Although the number of grid points for the TA grid is

Table 1 The smallest number of radial grid points with accuracy >15 for the electron-counting integrals of atoms H through to Kr using the TA, MK, DE1, DE2, and DE3 radial grids combined with Lebedev angular grid ($n^{\Omega} = 14$)

Atom	TA	MK	DE1	DE2	DE3
H	70	70	100	80	60
He	70	50	90	70	60
Li	90	130	110	90	100
Be	90	80	100	90	100
B	90	80	100	90	110
C	90	80	100	80	100
N	90	80	100	80	110
O	90	80	90	90	110
F	90	80	90	90	100
Ne	100	80	90	90	110
Na	120	160	110	110	150
Mg	110	100	110	100	140
Al	120	180	110	110	150
Si	120	120	110	100	140
P	120	90	100	100	140
S	120	100	90	100	130
Cl	120	100	90	100	140
Ar	120	110	100	100	130
K	150	NC[a] (13.8)[b]	120	120	170
Ca	130	150	110	110	150
Sc	140	NC[a] (11.2)[b]	100	110	160
Ti	170	NC[a] (12.3)[b]	110	110	160
V	160	NC[a] (12.1)[b]	100	110	150
Cr	130	NC[a] (12.6)[b]	100	100	170
Mn	130	NC[a] (13.7)[b]	110	110	160
Fe	140	NC[a] (13.7)[b]	100	110	160
Co	140	NC[a] (14.0)[b]	110	110	160
Ni	140	200	110	110	160
Cu	160	NC[a] (14.0)[b]	110	110	170
Zn	150	190	100	110	160
Ga	170	150	110	110	170
Ge	160	150	110	110	170
As	170	140	110	110	150
Se	160	160	110	110	170
Br	160	150	110	110	160
Kr	140	150	110	110	150

[a] Accuracy does not converge to 15 or higher at $n^r = 200$

[b] Values in parentheses are accuracy at $n^r = 200$

almost constant for the elements in each period except for the 4th period, the required number increases in the applications to atoms from light to heavy elements. As for the 4th-period elements with the TA grid, the convergence of accuracy depends on atomic species. The atoms of Ca, Cr, and Mn show the fastest convergence at $n^r = 130$, whereas the atoms of Ti, Ga, and As indicate the slowest convergence at $n^r = 170$. The dependence of the convergence behavior on atomic species is more remarkable for the MK grid than for the TA grid. The relative poor precision of the MK grid for transition metals at $n^r = 100$ remains also at $n^r = 200$ except for Ni. The accuracies of the MK grid do not reach the values of 15 or higher by using the grids up to $n^r = 200$ for the atoms of K, Sc, Ti, V, Cr, Mn, Fe, Co, and Cu. In addition, the accuracies of transition metals are much different with each other at $n^r = 200$ such as the lowest accuracy of 11.2 for Sc atom and the highest accuracy of 15.0 for Ni atom. The accuracies of Ti-Co atoms between Sc and Ni gradually vary from 12.3 to 14.0, indicating that the accuracies for transition metals of Sc–Ni change by about four orders of magnitude. On the other hand, the Cu atom results in the 14.0 accuracy which is lower than the Ni atom by one order of magnitude. Concerning the atoms with the converged accuracy, the MK integration also needs more grid points for the atoms of Li, Na, Al, Ni, and Zn than for the other

atoms in the same period. For the 2nd-period elements, the accuracy of Li atom converges at $n^r = 130$ in contrast to the other atoms converged at $n^r = 80$. The accuracy convergence requires the 160 and 180 points for Na and Al atoms, respectively, compared with about 100 points for the other atoms in the 3rd period. The Ni and Zn atoms show the converged accuracy by using the 200- and 190-point grids, respectively, whereas the other 4th-period atoms obtain the converged accuracy by using about 150-point grid. It is, therefore, necessary to add grid points more than about 50 points for the convergence of accuracy using the MK grid with respect to the specific atoms within the same period.

By the use of the DE1, DE2, and DE3 grids, the accuracies converge to the exact value at the following grid points for the elements in each period: 90–100 (1st period), 90–110 (2nd period), 90–110 (3rd period), and 100–120 (4th period) for the DE1 grid; 70–80 (1st period), 80–90 (2nd period), 100–110 (3rd period), and 100–120 (4th period) for the DE2 grid; 60 (1st period), 100–110 (2nd period), 130–150 (3rd period), and 150–170 (4th period) for the DE3 grid. The number of sampling points with the DE1, DE2, and DE3 grids is fairly invariable for every atom within the same period over the 1st, 2nd, 3rd, and 4th periods, indicating stable convergence property of the DE formula from a viewpoint of the sensitivity for the quadrature accuracy to atomic species. The variations of sampling points between the neighboring periods are also relatively small for the DE1 and DE2 grids. Consequently, the DE1 and DE2 schemes give the converged accuracy with the 120 or less grid points for all the atoms from H to Kr. On the other hand, the sampling points of the DE3 grid for heavy elements rather increase compared with the DE1 and DE2 grids up to 150 and 170 points for the 3rd- and 4th-period elements, respectively. The convergence rate for different-period atoms using each of the DE schemes tends to be DE3 > DE2 > DE1 (1st period), DE2 > DE1 > DE3 (2nd period), and DE1 $\approx$ DE2 > DE3 (3rd and 4th periods). Therefore, the DE3 grid converges more slowly than the DE1 and DE2 grids for the 3rd- and 4th-period elements.

The following characteristic features of the radial grids under a 10-point resolution of the grid size are found from the comparisons of the TA and MK results with the DE results. The increment of grid points from the 1st-period elements to the 4th-period elements is small for the DE1 and DE2 grids in contrast to the TA and MK grids. The results, thus, reveal that the convergence of the integrated values to the exact value is more stable for the DE1 and DE2 integrations with less dependence on atomic species than for the TA and MK integrations with more dependence on atomic species. Furthermore, the DE1 and DE2 grids converge faster than the TA and MK grids for the 4th-period elements. The DE3 grid requires a slightly large grid for the atoms in the 2nd and 3rd periods to obtain the converged accuracy in comparison with the TA and MK grids except for the Li, Na, and Al atoms using the MK grid. However, the differences of convergence behavior among the same-period atoms are much smaller in the case of the DE3 quadrature than in the case of the MK quadrature even for the 4th-period elements.

Here, we compare the convergence behavior of atomic integrals with that of molecular integrals to investigate relations between the performances of radial grids in the both cases. The electron-counting integrals of diatomic molecules including alkali metal and halogen of the 2nd, 3rd, and 4th periods were examined using the 6-31G** basis set in the preceding study [32]. The accuracy and convergence were reported for LiH, Li_2, HF, F_2, LiF (2nd period), NaH, Na_2, HCl, Cl_2, NaCl (3rd period), and KH, K_2, HBr, Br_2, KBr (4th period). However, the accuracies using the TA and MK grids for the molecules of LiH, LiF, NaH, NaCl, KH, and KBr with ionic bond resulted in poor precision lower than 15 even at $n^r = 200$ [32]. The TA and MK integrations for the molecules of Li_2, HF, F_2, Na_2, HCl, Cl_2, K_2, HBr, and Br_2 with covalent bond converged to the accuracy >15 by using the following grid points: 90–100 (2nd period), 120 (3rd period), and 150–170 (4th period) for the TA grid; 80 for HF and F_2 and 110 for Li_2 (2nd period), 100 for HCl and Cl_2 and 160 for Na_2 (3rd period), and 150–160 for HBr and Br_2 and 190 for K_2 (4th period) for the MK grid [32]. The convergence behavior of the TA and MK schemes shows similar trend for molecular integrals to atomic integrals described in the previous paragraph. The performance of the MK grid is also poor for the Li, Na, and K atoms in molecules. The DE1, DE2, and DE3 quadratures for all the diatomic molecules including alkali metal hydrides and alkali metal halogenides gave the converged accuracy to 15 or higher at the following grid points: 90–120 except for Li_2 and 150 for Li_2 (2nd period), 110–140 except for Na_2 and 160 for Na_2 (3rd period), and 130–150 except for K_2 and 180 for K_2 (4th period) for the DE1 grid; 110–130 (2nd period), 120–130 (3rd period), and 140–150 (4th period) for the DE2 grid; 110–120 (2nd period), 140–150 (3rd period), and 150–180 (4th period) for the DE3 grid [32]. The convergence behavior of the DE1 and DE2 grids is also more stable than that of the TA and MK grids even for molecular cases similar to atomic cases because of less dependence on atomic species, except for diatomic molecules of alkali metal with the DE1 grid. The atom-dependent performance of the DE3 grid found in atomic calculations is also observed in molecular calculations. It is, thus, confirmed that the accuracy of molecular integrals is affected by the characteristic feature of a radial grid for isolated atoms.

Tables 2, 3, 4, 5, and 6 summarize the performance of each radial grid for the TA, MK, DE1, DE2, and DE3 grids, respectively. The average value and standard deviation of accuracy over the elements in each period for the electron-counting integrals of atoms H through to Kr are given together with those over all the elements.

Although the 1st and the 4th periods show the fastest and the slowest convergences, respectively, among the 1st, 2nd, 3rd, and 4th periods in common with all the TA, MK, and DE grids, the convergence rate of the TA, MK, and DE3 schemes to the exact value significantly differs from that of the DE1 and DE2 schemes for the elements belonging to the different period as listed in Table 1. Such differences in convergence rate cause the inconsistent accuracy of quadrature approximation with the same-size grid for each period. The changes in average accuracy of the radial grids between the 1st and the 4th periods are obtained from Tables 2, 3, 4, 5, and 6. The maximum change of each grid is 6.8 for the TA grid at $n^r = 60$, 6.4 for the MK grid at $n^r = 60$ and 70, 2.5 for the DE1 grid at $n^r = 60$, 4.8 for the DE2 grid at $n^r = 70$, and 8.3 for the DE3 grid at $n^r = 60$. The accuracies of the TA and MK grids are much different by about seven and six orders of magnitude, respectively, for the atoms in these periods. The accuracy change for the DE1, DE2, and DE3 grids is about three, five, and eight orders of magnitude, respectively, indicating that the accuracy variation becomes small or large compared with the TA and MK grids by using the DE1 and DE2 grids or by using the DE3 grid. The accuracy difference reduces to less than one order of magnitude using the following- or larger-size grids except for the MK grid as 0.4 for the TA grid with 150 points, 1.2 for the MK grid with 200 points, 0.1 for the DE1 grid with 110 points, 0.2 for the DE2 grid with 110 points, and 0.8 for the DE3 grid with 150 points.

Consequently, the difference between accuracies for the different-period elements calculated using the same number of grid points becomes large if the grid size is not sufficiently large to give converged values for all the periods. It is, therefore, difficult to control the accuracy of numerical integration by the number of sampling points. The DE1 and DE2 schemes remarkably improve the accuracy control, since the integrated results rapidly converge to the exact value in nearly constant rate for every atom from H to Kr.

The qualitative trend regarding the points mentioned above is evaluated from the standard deviation of accuracy for each of the radial grids. If the convergence rate for each atom in a period is nearly constant, the standard deviation of the period gives nearly constant values for the variation of grid size. The standard deviation becomes 0.0 when the accuracies of the atoms finally converge to the same value. It is characteristic that the 4th-period standard deviations with the MK grid (1.4–1.8) are rather large in contrast to

Table 2 Average value and standard deviation of accuracy over the elements in each period (H–He, Li–Ne, Na–Ar, and K–Kr) and over all the elements (H–Kr) for the electron-counting integrals of atoms H through to Kr by the TA radial grid combined with Lebedev angular grid ($n^\Omega = 14$)

n^r	Average value					Standard deviation				
	1st	2nd	3rd	4th	Total	1st	2nd	3rd	4th	Total
30	9.3	6.5	5.9	4.6	5.6	0.4	0.4	0.2	0.3	1.2
40	12.4	7.8	6.5	6.7	7.2	0.2	0.4	0.2	0.8	1.5
50	13.7	9.1	8.0	7.2	8.2	0.5	0.4	0.6	0.6	1.6
60	14.9	10.7	8.7	8.1	9.2	0.0	0.3	0.1	0.3	1.7
70	15.7	12.4	9.9	9.0	10.3	0.0	0.7	0.2	0.5	1.9
80	15.6	14.0	11.3	9.5	11.3	0.1	0.5	0.7	0.2	2.1
90	15.4	15.2	12.3	10.5	12.2	0.0	0.3	0.2	0.4	2.0
100	15.5	15.4	13.9	11.5	13.1	0.3	0.2	0.4	0.5	1.8
110	15.6	15.6	14.7	12.3	13.7	0.1	0.2	0.2	0.8	1.6
120	15.7	15.6	15.4	13.0	14.3	0.0	0.1	0.3	0.7	1.4
130	15.7	15.6	15.5	13.9	14.7	0.0	0.2	0.2	0.9	1.1
140	15.7	15.6	15.5	14.5	15.0	0.0	0.2	0.3	0.7	0.7
150	15.3	15.6	15.4	14.9	15.2	0.1	0.1	0.2	0.5	0.5
160	15.6	15.5	15.6	15.2	15.4	0.1	0.2	0.2	0.4	0.3
170	15.6	15.5	15.4	15.4	15.4	0.1	0.2	0.2	0.3	0.3
180	15.6	15.2	15.6	15.5	15.5	0.1	0.1	0.1	0.3	0.2
190	15.3	15.4	15.5	15.5	15.4	0.2	0.3	0.1	0.3	0.2
200	15.3	15.5	15.3	15.5	15.4	0.1	0.2	0.3	0.3	0.3

Table 3 Average value and standard deviation of accuracy over the elements in each period (H–He, Li–Ne, Na–Ar, and K–Kr) and over all the elements (H–Kr) for the electron-counting integrals of atoms H through to Kr by the MK radial grid combined with Lebedev angular grid ($n^{\Omega} = 14$)

n^r	Average value					Standard deviation				
	1st	2nd	3rd	4th	Total	1st	2nd	3rd	4th	Total
30	9.2	7.0	7.0	5.8	6.5	0.8	0.5	0.5	0.6	1.0
40	11.5	8.6	7.3	6.8	7.5	1.1	0.4	0.3	0.4	1.3
50	13.9	10.4	8.6	8.1	9.1	1.5	0.8	0.3	0.5	1.6
60	14.8	11.9	9.8	8.4	9.9	0.9	0.8	0.5	0.4	1.9
70	15.7	13.7	10.8	9.3	11.0	0.0	0.9	0.7	0.6	2.2
80	15.5	15.0	12.1	9.8	11.8	0.0	1.1	0.9	0.7	2.4
90	15.7	15.1	13.5	10.5	12.5	0.0	0.9	1.2	1.1	2.3
100	15.7	15.4	14.2	10.9	12.9	0.0	0.6	1.4	0.9	2.3
110	15.7	15.4	14.7	11.4	13.2	0.0	0.3	1.4	1.1	2.2
120	15.6	15.4	14.9	11.8	13.5	0.1	0.3	1.2	1.2	2.0
130	15.6	15.5	15.0	12.4	13.8	0.1	0.1	0.9	1.4	1.8
140	15.6	15.6	15.3	12.9	14.2	0.1	0.2	0.6	1.5	1.7
150	15.4	15.6	15.2	13.3	14.4	0.3	0.2	0.5	1.8	1.6
160	15.6	15.4	15.5	13.6	14.5	0.1	0.3	0.5	1.7	1.6
170	15.4	15.6	15.3	13.7	14.6	0.3	0.1	0.3	1.6	1.4
180	15.7	15.5	15.5	13.9	14.7	0.0	0.2	0.2	1.5	1.3
190	15.6	15.7	15.5	14.1	14.8	0.1	0.1	0.2	1.4	1.2
200	15.5	15.7	15.4	14.3	14.9	0.0	0.1	0.2	1.4	1.2

Table 4 Average value and standard deviation of accuracy over the elements in each period (H–He, Li–Ne, Na–Ar, and K–Kr) and over all the elements (H–Kr) for the electron-counting integrals of atoms H through to Kr by the DE1 radial grid combined with Lebedev angular grid ($n^{\Omega} = 14$)

n^r	Average value					Standard deviation				
	1st	2nd	3rd	4th	Total	1st	2nd	3rd	4th	Total
30	5.5	4.8	5.0	4.9	4.9	0.2	0.3	0.5	0.5	0.5
40	7.0	6.7	6.1	6.5	6.5	0.6	0.4	0.4	0.4	0.5
50	9.7	8.2	7.8	7.9	8.1	1.4	0.9	0.5	0.4	0.8
60	11.8	10.0	9.1	9.3	9.6	0.2	0.6	0.3	0.4	0.8
70	12.6	11.3	11.1	10.9	11.1	0.4	0.9	0.6	0.4	0.7
80	14.5	13.0	12.2	12.5	12.7	0.4	1.1	0.6	0.7	0.9
90	15.3	14.5	14.0	13.4	13.9	0.4	1.0	1.2	0.5	1.0
100	15.7	15.4	14.9	14.7	15.0	0.0	0.6	0.6	0.6	0.7
110	15.6	15.5	15.4	15.5	15.5	0.1	0.2	0.2	0.3	0.2
120	15.7	15.6	15.4	15.6	15.6	0.0	0.2	0.2	0.2	0.2
130	15.7	15.5	15.6	15.6	15.6	0.0	0.2	0.1	0.2	0.2
140	15.7	15.7	15.5	15.5	15.6	0.0	0.1	0.1	0.2	0.2
150	15.7	15.6	15.5	15.6	15.6	0.0	0.1	0.2	0.2	0.2
160	15.6	15.6	15.6	15.6	15.6	0.1	0.1	0.2	0.2	0.2
170	15.7	15.5	15.5	15.6	15.5	0.0	0.2	0.2	0.2	0.2
180	15.4	15.5	15.6	15.6	15.5	0.2	0.2	0.2	0.2	0.2
190	15.7	15.6	15.4	15.5	15.5	0.0	0.1	0.2	0.2	0.2
200	15.5	15.6	15.6	15.5	15.6	0.3	0.1	0.2	0.2	0.2

Table 5 Average value and standard deviation of accuracy over the elements in each period (H–He, Li–Ne, Na–Ar, and K–Kr) and over all the elements (H–Kr) for the electron-counting integrals of atoms H through to Kr by the DE2 radial grid combined with Lebedev angular grid ($n^{\Omega} = 14$)

n^r	Average value					Standard deviation				
	1st	2nd	3rd	4th	Total	1st	2nd	3rd	4th	Total
30	5.8	5.0	4.6	3.9	4.4	0.1	0.6	0.3	0.3	0.7
40	8.0	7.2	6.4	5.6	6.3	0.0	0.7	0.8	0.3	0.9
50	10.6	9.2	7.9	7.3	8.0	0.1	0.4	0.5	0.6	1.1
60	13.0	10.9	10.0	8.9	9.8	0.6	0.6	0.4	0.6	1.3
70	15.2	12.5	11.2	10.4	11.3	0.3	0.4	0.7	0.7	1.4
80	15.6	14.7	12.7	12.2	13.0	0.1	0.4	0.2	0.7	1.3
90	15.6	15.5	14.1	13.1	14.0	0.1	0.1	0.3	0.4	1.1
100	15.6	15.5	15.2	14.3	14.9	0.1	0.2	0.3	0.3	0.6
110	15.6	15.7	15.7	15.4	15.5	0.1	0.1	0.1	0.3	0.2
120	15.6	15.7	15.6	15.6	15.6	0.1	0.1	0.1	0.1	0.1
130	15.6	15.6	15.6	15.6	15.6	0.1	0.2	0.2	0.2	0.2
140	15.4	15.6	15.6	15.5	15.5	0.3	0.1	0.1	0.2	0.2
150	15.5	15.7	15.7	15.6	15.6	0.3	0.0	0.0	0.2	0.2
160	15.7	15.5	15.6	15.6	15.6	0.0	0.2	0.2	0.1	0.2
170	15.6	15.5	15.4	15.4	15.5	0.1	0.2	0.2	0.2	0.2
180	15.6	15.5	15.5	15.6	15.5	0.1	0.2	0.2	0.2	0.2
190	15.6	15.5	15.5	15.5	15.5	0.1	0.2	0.2	0.2	0.2
200	15.7	15.6	15.4	15.5	15.5	0.0	0.1	0.2	0.2	0.2

Table 6 Average value and standard deviation of accuracy over the elements in each period (H–He, Li–Ne, Na–Ar, and K–Kr) and over all the elements (H–Kr) for the electron-counting integrals of atoms H through to Kr by the DE3 radial grid combined with Lebedev angular grid ($n^{\Omega} = 14$)

n^r	Average value					Standard deviation				
	1st	2nd	3rd	4th	Total	1st	2nd	3rd	4th	Total
30	8.0	5.7	4.0	3.8	4.5	0.3	0.3	0.3	0.3	1.2
40	10.9	6.4	5.9	4.5	5.6	0.5	0.2	0.8	0.2	1.6
50	13.4	8.3	6.7	6.3	7.2	0.4	0.3	0.3	0.6	1.7
60	15.7	9.0	7.6	7.4	8.2	0.0	0.1	0.4	0.6	2.0
70	15.7	10.3	8.6	8.0	9.1	0.0	0.2	0.2	0.5	1.9
80	15.7	11.7	9.6	8.8	10.0	0.0	0.2	0.5	0.4	1.8
90	15.4	13.0	10.9	9.4	10.9	0.0	0.2	0.9	0.5	1.9
100	15.6	14.7	11.5	10.9	12.2	0.1	0.7	0.5	0.6	1.8
110	15.6	15.5	12.6	11.3	12.7	0.1	0.2	0.4	0.4	1.8
120	15.7	15.6	13.8	12.3	13.5	0.0	0.1	0.7	0.4	1.5
130	15.4	15.5	14.4	12.9	13.9	0.0	0.2	0.5	0.4	1.2
140	15.7	15.6	15.3	13.4	14.4	0.0	0.1	0.4	0.3	1.1
150	15.4	15.5	15.6	14.6	15.1	0.2	0.2	0.2	0.5	0.6
160	15.6	15.6	15.6	15.0	15.3	0.1	0.2	0.1	0.3	0.4
170	15.5	15.5	15.5	15.5	15.5	0.3	0.2	0.2	0.2	0.2
180	15.7	15.5	15.4	15.6	15.5	0.0	0.2	0.3	0.2	0.2
190	15.7	15.6	15.5	15.5	15.6	0.0	0.2	0.2	0.2	0.2
200	15.4	15.5	15.5	15.4	15.4	0.3	0.2	0.3	0.2	0.2

those with the other grids (0.2–0.5) even if the large-size grids of 150 or more points are used, since there exist both the atoms that converge to high accuracy or stay low precision within the period in the case of the MK grid.

The improvements of accuracy by adding the sampling points of numerical integration delay from light to heavy elements as found in the average accuracy for each period of Tables 2, 3, 4, 5, and 6. Therefore, first the accuracy dispersion over all the atoms increases compared with the starting grid of 30 points and then decreases with appearing the converged atoms to the exact value. Total standard deviation of the TA and DE3 grids with the values larger than 1.0 is distributed from 1.1 to 2.1 for $n^r = 30$–130 and from 1.1 to 2.0 for $n^r = 30$–140, respectively. The MK grid has total standard deviation ranging from 1.0 to 2.4 over all the grid sizes of $n^r = 30$–200 due to poor precision for the 4th-period elements in average. These results elucidate large dispersion of the accuracy for these grids. On the other hand, total standard deviation of the DE1 and DE2 grids is obtained as the values from 0.5 to 1.0 (DE1) and from 0.6 to 1.4 (DE2) for $n^r = 30$–100. It is clearly confirmed that the dispersion of accuracy for the sparse grids that give non-converged results is smaller for the DE1 and DE2 grids than for the TA, MK, and DE3 grids. The DE1 and DE2 grids show very small dispersion of accuracy in wide range of the grid size owing to fast convergence with similar rate for all the atoms such that total standard deviation is less than 0.2 for $n^r = 110$–200.

The results of numerical integration vary depending on the mapping parameter α. The α value can be optimized for each atom. However, we did not tune the DE radial grids to individual atom. The α values for the DE1, DE2, and DE3 grids were simply determined on the basis of averaged accuracy over all of different-size grids and all of atomic species as the common values of 2.4 (DE1), 1.9 (DE2), and 2.3 (DE3) to all the atoms. Although these α values are not optimal, the DE grids demonstrate good performance. To clarify the dependence of performance on the mapping parameter for the DE formula, the changes in average accuracy for the mapping parameter ranging from $\alpha-1.0$ to $\alpha+1.0$ are illustrated in Figs. 2, 3 and 4 for the DE1, DE2, and DE3 grids, respectively. The average of accuracy for the electron-counting integrals of atoms H trough to Kr is taken over each of the 1st-, 2nd-, 3rd-, and 4th-period elements (H–He, Li–Ne, Na–Ar, and K–Kr). For clear view, the results obtained with the selected grid sizes of $n^r = 30$, 50, 70, 100, 150, and 200 are plotted. The variation ranges in average accuracy and standard deviation using $n^r = 30$ to 200 are also fully listed in Online Resources 6, 7, and 8 for each radial grid as Table S6 for the DE1 grid, Table S7 for the DE2 grid, and Table S8 for the DE3 grid, respectively.

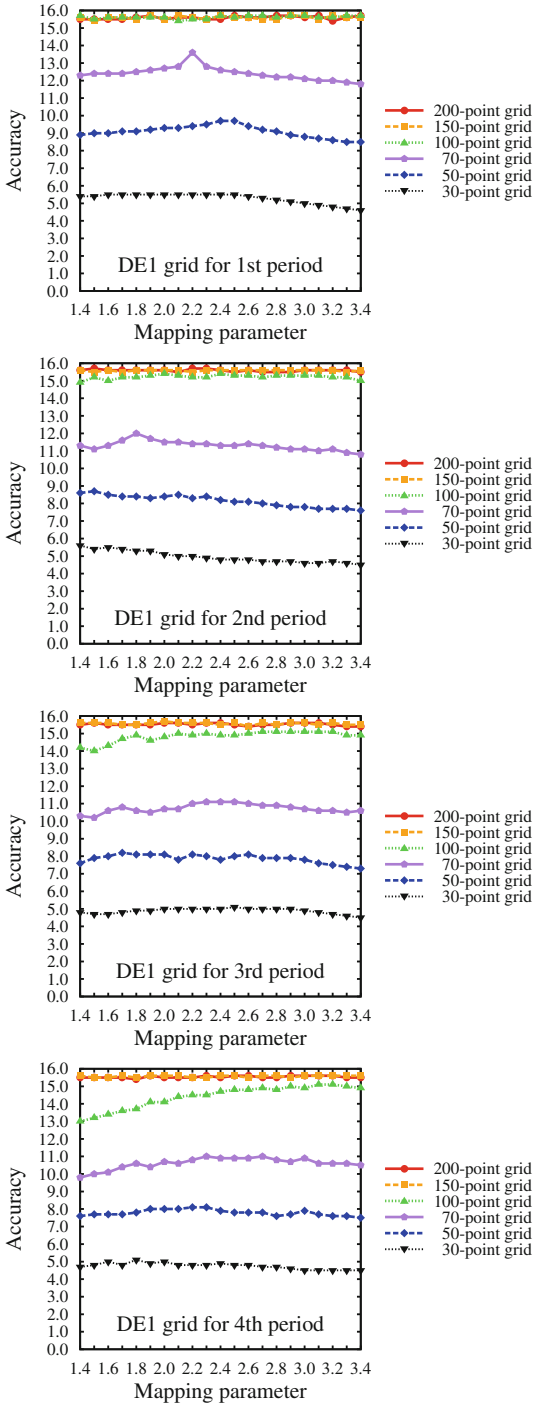

Fig. 2 Changes in average accuracy of the DE1 radial grid combined with Lebedev angular grid ($n^\Omega = 14$) for the electron-counting integrals of the 1st-, 2nd-, 3rd-, and 4th-period elements (H–He, Li–Ne, Na–Ar, and K–Kr)

The changes in average accuracies for the DE1, DE2, and DE3 grids are fairly stable (flat) in wide range with respect to the variation of the mapping parameter. In particular, the accuracy of the DE1 grid is not sensitive to the

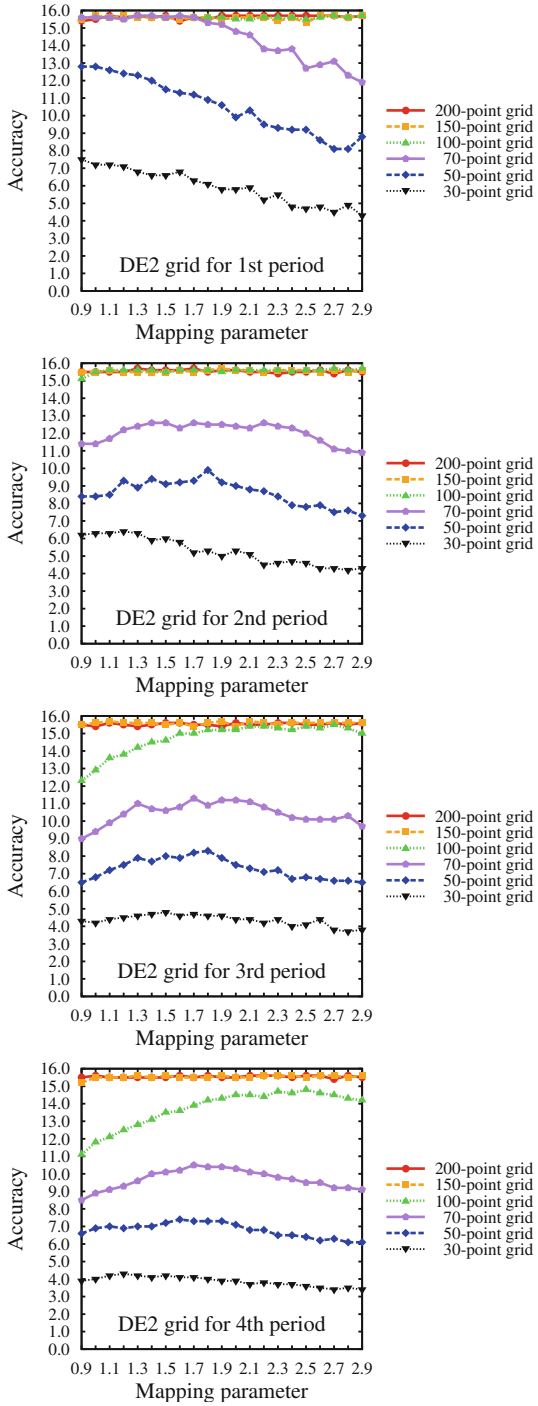

Fig. 3 Changes in average accuracy of the DE2 radial grid combined with Lebedev angular grid ($n^{\Omega} = 14$) for the electron-counting integrals of the 1st-, 2nd-, 3rd-, and 4th-period elements (H–He, Li–Ne, Na–Ar, and K–Kr)

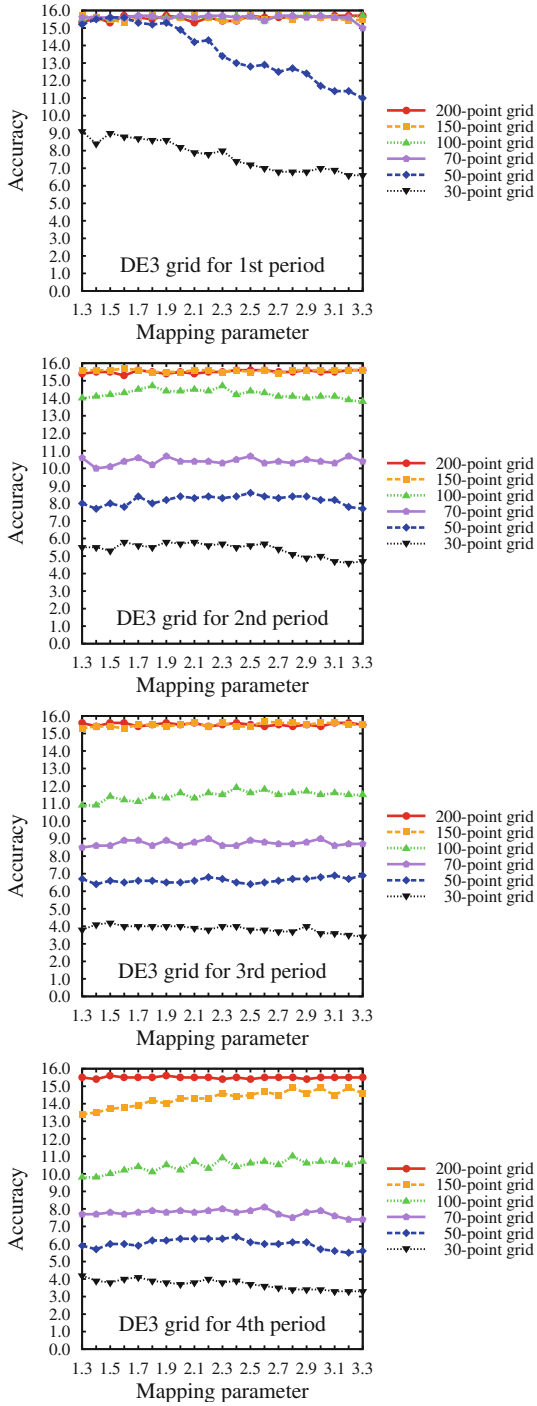

Fig. 4 Changes in average accuracy of the DE3 radial grid combined with Lebedev angular grid ($n^{\Omega} = 14$) for the electron-counting integrals of the 1st-, 2nd-, 3rd-, and 4th-period elements (H–He, Li–Ne, Na–Ar, and K–Kr)

α value for every period. The DE2 and DE3 calculations for the 1st-period elements result in higher accuracy for small α value than for large α value. The DE2 grid for the 3rd- and 4th-period elements tends to be less precise when the α value is small. The DE2 results of the 2nd period and the DE3 results of the 2nd, 3rd, and 4th periods give relatively flat accuracy.

If we determine the value of the mapping parameter by averaging the accuracy over the elements in each period instead of all the atoms, the following α values are

obtained: 2.4 (1st period), 1.8 (2nd period), 2.3 (3rd period), and 2.4 (4th period) for the DE1 grid; 0.8 (1st period), 1.8 (2nd period), 1.8 (3rd period), and 1.9 (4th period) for the DE2 grid; 1.8 (1st period), 2.1 (2nd period), 2.4 (3rd period), and 2.8 (4th period) for the DE3 grid. The α values for the 2nd period of the DE1 grid, the 1st period of the DE2 grid, and the 1st–4th periods of the DE3 grid are different from those for the other periods of the same DE grid. The α values with the average accuracy over all the atoms are 2.4, 1.9, and 2.3 for the DE1, DE2, and DE3 grids, respectively, as mentioned in Sect. 3. The average accuracies of the DE1 grid for the 2nd-period elements and the DE3 grid for the 2nd-, 3rd-, and 4th-period elements are relatively invariant from $\alpha = 1.8$ to $\alpha = 2.4$ (DE1 grid) and from $\alpha = 2.1$ to $\alpha = 2.8$ (DE3 grid). Since the accuracy changes are within one order of magnitude, the influences by using $\alpha = 2.4$ instead of $\alpha = 1.8$ for the 2nd period (DE1 grid) and $\alpha = 2.3$ instead of $\alpha = 2.1$, 2.4, 2.8 for the 2nd–4th periods (DE3 grid) are small. The average accuracies of the DE2 and DE3 grids for the 1st-period elements become more precise for $\alpha = 0.8$ than for $\alpha = 1.9$ (DE2 grid) and for $\alpha = 1.8$ than for $\alpha = 2.3$ (DE3 grid) in the cases of small-size grids with the 30–60 points (DE2 grid) and the 30–50 points (DE3 grid). Since the accuracies of these sparse grids are improved by about two orders of magnitude, the convergence of accuracy is accelerated by applying the α values specific to the 1st period. Although the use of suitable mapping parameters for each period or each atom will somewhat improve the performance, the DE grids with single mapping parameter sufficiently work well as demonstrated in the present study.

We have reported in the preceding study [32] that the DE1 and DE2 schemes using single mapping parameter are useful to integrate the molecular electron density for diatomic molecules containing the Li, Na, K, F, Cl, Br, Sc, Mn, and Cu atoms. We elucidate in the present study that the similar accuracy and convergence rate of the integrated results is achieved by applying the DE1 and DE2 schemes to other atoms for the integration of atomic electron density. Therefore, the DE1 and DE2 grids are expected to be also useful for molecules composed of other atoms.

5 Concluding remarks

In this study, we investigated the performance of the DE formula on the numerical integration of the radial electron distribution function represented with the GTO basis functions for atomic systems. Three-type DE transformations were applied to generate new radial quadrature grids referred to as the DE1, DE2, and DE3 grids. The accuracy and convergence of the DE grids were compared with those of the TA and MK grids proposed in earlier studies for the electron-counting integrals of atoms H through to Kr. We also demonstrated the dependence of the DE results on the variation of the mapping parameter for the elements from the 1st period to the 4th period.

The integrated values converge to the exact value fast by using the DE1 and DE2 quadratures. Particularly, rapid convergence of the DE1 and DE2 integrations is attained in contrast to poor convergence of the TA and MK integrations even for the 4th-period elements. Furthermore, it is demonstrated that the convergence rate of the DE1 and DE2 grids is nearly constant over the elements of different periods compared with the atom-dependent convergence rate of the TA and MK grids. Thus, the DE1 and DE2 grids show similar or higher accuracies in average compared with the TA and MK grids especially for the 4th-period elements. The dispersion of accuracy obtained with the same grid size for all the atoms becomes smaller in the DE1 and DE2 results than in the TA and MK results. The DE1 and DE2 schemes give stable performance for all the atoms compared with the TA and MK schemes. On the other hand, the DE3 grid is less efficient than the DE1 and DE2 grids, since the convergence depends on atomic species similar to the TA and MK grids.

Judging from the results obtained in this study, the DE1 and DE2 radial grids are considered to be superior to the TA and MK radial grids from a viewpoint that the accuracy is less sensitive to grid sizes and atomic species. The sweet spot of the mapping parameter is also wide for the DE radial grids. Consequently, it is reasonable to expect that the DE1 and DE2 schemes are useful to improve the reliability and efficiency for the numerical integration of energy functionals associated with heavy elements in density functional calculations by combining with an accurate angular grid and an appropriate nuclear weight function for molecular integrals. We will confirm the performance of the DE formula for the energy functionals in the future studies.

References

1. Becke AD (1988) J Chem Phys 88:2547–2553
2. Lebedev VI (1975) Comp Math Math Phys 15:44–51
3. Lebedev VI (1976) Comp Math Math Phys 16:10–24
4. Lebedev VI (1977) Sib Math J 18:99–107
5. Lebedev VI, Skorokhodov AL (1992) Russ Acad Sci Dokl Math 45:587–592
6. Lebedev VI (1995) Russ Acad Sci Dokl Math 50:283–286
7. Lebedev VI, Laikov DN (1999) Dokl Math 59:477–481
8. Murray CW, Handy NC, Laming GJ (1993) Mol Phys 78:997–1014
9. Gill PMW, Johnson BG, Pople JA (1993) Chem Phys Lett 209:506–512
10. Pérez-Jordá JM, Becke AD, San-Fabián E (1994) J Chem Phys 100:6520–6534

11. Treutler O, Ahlrichs R (1995) J Chem Phys 102:346–354
12. Mura ME, Knowles PJ (1996) J Chem Phys 104:9848–9858
13. Krack M, Köster AM (1998) J Chem Phys 108:3226–3234
14. Lin Z, Jaffe JE, Hess AC (1999) J Phys Chem A 103:2117–2127
15. Ishikawa H, Yamamoto K, Fujima K, Iwasawa M (1999) Int J Quantum Chem 72:509–523
16. Lindh R, Malmqvist P-Å, Gagliardi L (2001) Theor Chem Acc 106:178–187
17. Gill PMW, Chien S-H (2003) J Comput Chem 24:732–740
18. Köster AM, Flores-Moreno R, Reveles JU (2004) J Chem Phys 121:681–690
19. Weber V, Daul C, Baltensperger R (2004) Comput Phys Comm 163:133–142
20. Kakhiani K, Tsereteli K, Tsereteli P (2009) Comput Phys Comm 180:256–268
21. El-Sherbiny A, Poirier RA (2004) J Comput Chem 25:1378–1384
22. Chien S-H, Gill PMW (2006) J Comput Chem 27:730–739
23. Martin JML, Bauschlicher CW Jr, Ricca A (2001) Comput Phys Comm 133:189–201
24. Johnson ER, Wolkow RA, DiLabio GA (2004) Chem Phys Lett 394:334–338
25. Papas BN, Schaefer HF III (2006) J Mol Struct Theochem 768:175–181
26. Takahashi H, Mori M (1974) Publ RIMS Kyoto Univ 9: 721–741 Journal@rchive, Japan Science and Technology Agency (JST). http://www.journalarchive.jst.go.jp/english/jnltop_en.php?cdjournal=kyotoms1969. Accessed 2 Sept 2011
27. Mori M (1985) J Comput Appl Math 12, 13: 119–130
28. Mori M, Sugihara M (2001) J Comput Appl Math 127:287–296
29. Muhammad M, Mori M (2003) J Comput Appl Math 161:431–448
30. Mori M (2005) Publ RIMS Kyoto Univ 41: 897–935 Publications of the Research Institute for Mathematical Sciences, Research Institute for Mathematical Sciences, Kyoto University. http://www.kurims.kyoto-u.ac.jp/~prims/list.html. Accessed 2 Sept 2011
31. Tanaka K, Sugihara M, Murota K, Mori M (2009) Numer Math 111:631–655
32. Mitani M (2011) Theor Chem Acc 130:645–669
33. Bunge CF, Barrientos JA, Bunge AV (1993) At Data Nucl Data Tables 53:113–162
34. Becke AD (1993) J Chem Phys 98:5648–5652
35. Lee C, Yang W, Parr RG (1988) Phys Rev B 37:785–789
36. Ditchfield R, Hehre WJ, Pople JA (1971) J Chem Phys 54:724–728
37. Hehre WJ, Ditchfield R, Pople JA (1972) J Chem Phys 56:2257–2261
38. Hariharan PC, Pople JA (1973) Theor Chim Acta 28:213–222
39. Hariharan PC, Pople JA (1974) Mol Phys 27:209–214
40. Gordon MS (1980) Chem Phys Lett 76:163–168
41. Francl MM, Petro WJ, Hehre WJ, Binkley JS, Gordon MS, DeFrees DJ, Pople JA (1982) J Chem Phys 77:3654–3665
42. Binning RC Jr, Curtiss LA (1990) J Comput Chem 11:1206–1216
43. Blaudeau J-P, McGrath MP, Curtiss LA, Radom L (1997) J Chem Phys 107:5016–5021
44. Rassolov VA, Pople JA, Ratner MA, Windus TL (1998) J Chem Phys 109:1223–1229
45. Rassolov VA, Ratner MA, Pople JA, Redfern PC, Curtiss LA (2001) J Comput Chem 22:976–984
46. Schäfer A, Horn H, Ahlrichs R (1992) J Chem Phys 97:2571–2577
47. Frisch MJ, Trucks GW, Schlegel HB, Scuseria GE, Robb MA, Cheeseman JR, Montgomery JA Jr, Vreven T, Kudin KN, Burant JC, Millam JM, Iyengar SS, Tomasi J, Barone V, Mennucci B, Cossi M, Scalmani G, Rega N, Petersson GA, Nakatsuji H, Hada M, Ehara M, Toyota K, Fukuda R, Hasegawa J, Ishida M, Nakajima T, Honda Y, Kitao O, Nakai H, Klene M, Li X, Knox JE, Hratchian HP, Cross JB, Adamo C, Jaramillo J, Gomperts R, Stratmann RE, Yazyev O, Austin AJ, Cammi R, Pomelli C, Ochterski JW, Ayala PY, Morokuma K, Voth GA, Salvador P, Dannenberg JJ, Zakrzewski VG, Dapprich S, Daniels AD, Strain MC, Farkas O, Malick DK, Rabuck AD, Raghavachari K, Foresman JB, Ortiz JV, Cui Q, Baboul AG, Clifford S, Cioslowski J, Stefanov BB, Liu G, Liashenko A, Piskorz P, Komaromi I, Martin RL, Fox DJ, Keith T, Al-Laham MA, Peng CY, Nanayakkara A, Challacombe M, Gill PMW, Johnson B, Chen W, Wong MW, Gonzalez C, Pople JA (2003) Gaussian 03, Revision B.05, Gaussian, Inc., Pittsburgh, PA